On the cost of electrodialysis for the desalination of high salinity feeds

Citation: McGovern, Ronan K., Adam M. Weiner, Lige Sun, Chester G. Chambers, Syed M. Zubair, and John H. Lienhard V. "On the Cost of Electrodialysis for the Desalination of High Salinity Feeds." Applied Energy 136 (December 2014): 649–661.

As Published: http://dx.doi.org/10.1016/j.apenergy.2014.09.050

Publisher: Elsevier

Persistent URL: http://hdl.handle.net/1721.1/105367

Version: Author's final manuscript: final author's manuscript post peer review, without publisher's formatting or copy editing

On the cost of electrodialysis for the desalination of high salinity feeds

On the cost of electrodialysis for the desalination of high salinity feeds

Ronan K. McGovern[a], Adam M. Weiner[a], Lige Sun[a], Chester G. Chambers[a], Syed M. Zubair[b], John H. Lienhard V[a]

[a] *Center for Clean Water and Clean Energy, Massachusetts Institute of Technology, Cambridge, MA 02139, U.S.A.*
[b] *King Fahd University for Petroleum and Minerals, Dhahran, Saudi Arabia*

Abstract

We propose the use of electrodialysis to desalinate produced waters from shale formations in order to facilitate water reuse in subsequent hydraulic fracturing processes. We focus on establishing the energy and equipment size required for the desalination of feed waters containing total dissolved solids of up to 192,000 ppm, and we do this by experimentally replicating the performance of a 10-stage electrodialysis system. We find that energy requirements are similar to current vapour compression desalination processes for feedwaters ranging between roughly 40,000-90,000 TDS, but we project water costs to potentially be lower. We also find that the cost per unit salt removed is significantly lower when removed from a high salinity stream as opposed to a low salinity stream, pointing towards the potential of ED to operate as a partial desalination process for high salinity waters. We then develop a numerical model for the system, validate it against experimental results and use this model to minimise salt removal costs by optimising the stack voltage. We find that the higher the salinity of the water from which salt is removed the smaller should be the ratio of the electrical current to its limiting value. We conclude, on the basis of energy and equipment costs, that electrodialysis processes are potentially feasible for the desalination of high salinity waters but require further investigation of robustness to fouling under field conditions.

Keywords: electrodialysis, desalination, brine concentration, energy efficiency, hydraulic fracturing, shale

1. Introduction

We have experimentally investigated factors affecting the cost of electrodialysis (ED) for the desalination of high salinity feeds, focusing on the dependence of the cost of salt removal upon diluate salinity. We have also developed a numerical model for the system, validated it against the experimental results and identified a strategy to optimise the stack voltage such that the sum of equipment and energy costs are minimised. Our motivation for this investigation was the desalination of produced waters in unconventional oil and gas extraction where, amongst other factors, the presence of high levels of total dissolved solids can disincentivise water reuse. Water reuse in hydraulic fracturing is of great interest both from an environmental perspective, as it reduces water use and minimises disposal through deep-well injection, but also from an economic perspective as water management costs can account for between 5 and 15% of drilling costs [1].

For the purpose of this investigation, we were most interested in flows of water during the life-cycle of a well, which are depicted in Fig. 1. For reuse to be economical, the savings in the sourcing, disposal and

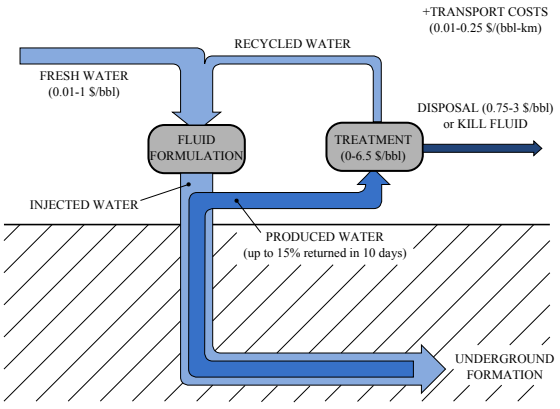

Figure 1: Fresh water [1] is mixed with recycled water and chemicals are added, that may include acids, friction reducers, gelling agents and proppant (sand) [2] to form the hydraulic fracturing fluid. The fluid is then injected into the well at high pressure to create fractures in the underlying shale formation. A portion of this fluid [3], perhaps in addition to fluid originally contained in the formations, subsequently returns to the surface, at a rate that generally decreases with time, and is known as produced water. The produced water may be: subjected to levels of treatment that vary from suspended solids removal to complete desalination [1] and recycling; sent to a disposal well; and/or employed elsewhere as a kill fluid (a fluid used to close off a well after production is complete) or as a salt based drilling fluid [1].

Email addresses: mcgov@alum.mit.edu (Ronan K. McGovern), lienhard@mit.edu (John H. Lienhard V)

R.K. McGovern, A.M. Weiner, L. Sun, C.G. Chambers, S.M. Zubair, and J.H. Lienhard V, “On the cost of electrodialysis for the desalination of high salinity feeds,” Applied Energy, 136:649-661, Dec. 2014

transport of water must outweigh any increased costs of treatment or of chemicals in the formulation of the fracturing fluid. This means that regional differences in recycling rates are strongly influenced by regional differences in sourcing, disposal and transport costs. For example, reuse rates are currently greatest in the Marcellus shales [3] (reused water makes up 10-15% of water needed to fracture a well) where transport and disposal costs can reach \$15-18/bbl (\$94-113/m^3) [4]. The initial rate at which produced water flows to the surface (e.g. within the first 10 days) also influences the viability of reuse as low initial produced water volume flow rates making the logistics of reuse more difficult [3, 5].

Moving to the costs of reuse, and setting aside the expense associated with logistics, the costs come primarily in the form of: increased water treatment costs; increased chemical costs in the formulation of the hydraulic fracturing fluid to mitigate undesirable feed water properties; and/or reduced oil or gas production from the well. By and large, the increase in treatment costs is highest, and the increase in chemical costs lowest, when produced water is treated with mechanical vapour compression. Vapour compression provides high purity water for the formulation of the hydraulic fracturing fluid but is expensive. Ranges of roughly 5-8 kWh/bbl (32-50 kWh/m^3) of distillate[1] [7] and 3.50-6.25 \$/bbl (\$22-39/m^3) of distillate [1] have been reported for the treatment of produced waters. While vapour compression provides a high purity feed for the formulation of the hydraulic fracturing fluid, direct reuse, whereby produced water is directly blended with freshwater before formulation of the fracturing fluid, results, by and large, in the lowest treatment costs but greater chemical costs for fluid formulation and perhaps a decline in the well's production. Increased costs associated with reuse, depending on the degree of treatment employed, can come in the form of: increased friction reducer and scale inhibitor demand with high chloride contents; increased scaling within the shale formation with the presence of divalent ions; increased corrosion of pipes; increased levels of sulphate reducing bacteria resulting in the production of H_2S gas [8]; and a reduction in the performance of coagulation/flocculation, flotation, gravity settling and plate and frame dewatering equipment due to residual unbroken polymer gel [9].

Many of the challenges faced in reuse can be dealt with through primary treatment that removes suspended solids, oil, iron, unbroken polymers and bacteria [9], generally at a cost much below complete desalination (circa \$1/bbl (\$6.3/m^3) compared to \$3.50-6.25/bbl (\$22-39/m^3) for complete desalination [1]). The need for the removal of all solids, suspended and dissolved, is less clear. Opinions vary as to the level of total dissolved solids (TDS) that can be tolerated [10] and a complete understanding of issues of chemical compatibility remains elusive [2]. There is evidence that, with improved chemical formulations, high salinity produced waters may be reused without desalination, particularly in the formulation of fluids for slickwater processes [11–16] (processes with high volume flow rates to avoid premature settling of sand, which serves to maintain fractures propped open) and to some extent for cross-linked gel fracturing processes [17] (lower volume flow rate processes employing low molecular weight guar gum based gels to ensure proppant remains suspended). However, the increase in chemical costs associated with such formulations not evident. Depending on the fracturing fluid desired, chemical use can be significant. Fedotov et al. [9] indicated that the use of drag reducing agents in slickwater fracturing processes, can reach approximately 1,000 ppm (2 lbs per 1,000 gallons), while for cross-linked gel fracturing processes chemical use can be much higher and reach 15,000 ppm (30 lbs/1,000 gallons).

In place of a distillation process, we propose the use of electrodialysis desalination to partially desalt produced water. The objective is to achieve a configuration that can reduce water treatment costs relative to distillation, by avoiding complete desalination, but can provide the benefit of reduced total dissolved solids relative to a direct reuse configuration. At present, a clear illustration of the dependence of ED salt removal costs on feed salinity is not present in literature, particularly for feed salinities above brackish. A number of studies consider seawater desalination with electrodialysis [18], including electrodialysis-reverse osmosis hybrid configurations [19], but focus upon energy costs alone. Lee et al. [20] consider the effect of feed salinity upon the cost of water from a continuous, as opposed to batch, electrodialysis system for brackish feed waters, McGovern et al. [21] analyse the dependence of water costs upon feed and product salinity in their analysis of hybrid ED-RO systems for brackish applications. Few studies exist that analyse both energy and capital costs for higher salinity feeds [22]. Batch studies of low salinity produced waters report energy consumption figures of 1.1 kWh/m^3 for 90% TDS removal and 0.36 kWh/m^3 for 50% TDS removal from a 3,000 ppm TDS stream [23]. A study at higher feed water salinity reports energy consumption of 12.4 kWh/m^3 for 80,000 ppm TDS [24]. A number of experimental studies, with desalination occurring in a batch mode, report the process times required to achieve a final target purity as increasing with the feed salinity [25, 26] but leave unclear how process times translate into equipment costs. Furthermore, energy consumption in batch processes is often reported as an average kWh/kg salt removed for an entire pro-

[1] 6.4 kWh/bbl (40 kWh/m^3) has been reported for 72.5% recovery of feedwater with total dissolved solids of 50,000 mg/L [6]

cess without focusing on how this value varies depending upon the diluate, and to a lesser extent the concentrate, salinity.

In this work, we conduct multiple stages of batch desalination on an experimental electrodialysis setup such that each stage replicates closely a stage within a continuous process. Furthermore, we relate batch process times and energy consumptions to the production rate and specific energy consumption that would be achieved from an equivalent continuous system. Coupled with a simple financial model, these metrics allow us to investigate and optimise the dependence of cost upon the feed salinity to a continuous electrodialysis system.

2. Methods

2.1. Experimental

We performed an experiment to replicate the performance of a ten stage continuous flow electrodialysis system capable of desalinating a feed stream from 224 mS/cm (195,000 ppm TDS NaCl) down to 0.5 mS/cm (240 ppm TDS NaCl). We studied aqueous NaCl solutions since Na^+ and Cl^- ions account for the vast majority of dissolved solids contained within produced water samples taken from the Barnett, Eagleford, Fayetteville, Haynesville, Marcellus and Bakken shale plays [1]. Thus, the electrical conductivity and chemical activity of salts in produced water samples – both important influencers of the energy consumption and system size in electrodialysis – are well simulated by aqueous NaCl solutions of matching total dissolved solids. To do this, we ran ten batch experiments, each representing a single stage in a continuous process. We chose the diluate conductivities at the start of each stage such that the diluate conductivity was halved in each stage and the salt removal was approximately 50% per stage [20] (see Fig. 2). We chose the concentrate concentration in each stage to replicate the concentration that would prevail if the concentrate salinity were to be determined solely by the rates of salt and water transport across the membranes (see Appendix A.1). We held the stack voltage constant at 8 V in all stages and chose this value such that the current density at the end of the final stage would be 50% of its limiting value (see Appendix A.2).

The experimental apparatus, illustrated in Fig. 3 involved an ED200 stack [27] with 17 cell pairs consisting of seventeen Neosepta AMS-SB, eighteen CMS-SB membranes, thirty-four 0.5 mm spacers and two 1 mm end spacers. We employed a GW Instek GPR-60600 and an Extech 382275 power supply to provide current in the ranges of 0-5 A and 5-20 amps respectively. We measured conductivity on a Jenco 3250 conductivity meter interfacing with model 106L (cell constant, K=1) and model 107N (cell constant, K=10) probes. We performed experiments in constant voltage mode, with current measured by an Extech EX542 multimeter. We determined initial diluate and concentrate volumes by summing the initial fluid volumes contained within the beakers (1 litre and 3 litres for the diluate and concentrate, respectively, in all tests) with the internal volumes of the diluate and concentrate fluid circuits (see Appendix A.3). We determined changes in diluate mass by tracking the mass of the diluate within the beaker using an Ohaus Scout Pro balance with a range of 0-2 kg. Changes in density were also accounted for given knowledge of solution conductivities versus time.

To quantify performance we considered certain key performance metrics. The first metrics are specific process times, based on stage salt removal, τ_i^s, and final stage diluate volume, τ_i^w:

$$\tau_i^s = \frac{t_i}{\left(V_i^{in,d} C_i^{in,d} - V_i^{f,d} C_i^{f,d}\right)} \tag{1}$$

$$\tau_i^w = \frac{t_i}{V_i^{f,d}} \tag{2}$$

where t_i is the process time for stage i, $V_i^{in,d}$ and $V_i^{f,d}$ are the initial and final stage volumes, and $C_i^{in,d}$ and $C_i^{f,d}$ are the initial and final stage concentrations. The second metrics are specific energy consumption, based on stage salt removal, E_i^s, and final stage diluate volume, E_i^w:

$$E_i^s = \frac{\sum_j I_{i,j} V_{i,j} \Delta t_{i,j}}{\left(V_i^{in,d} C_i^{in,d} - V_i^{f,d} C_i^{f,d}\right)} \tag{3}$$

$$E_i^w = \frac{\sum_j I_{i,j} V_{i,j} \Delta t_{i,j}}{V_i^{f,d}} \tag{4}$$

where $I_{i,j}$ and $V_{i,j}$ are the stack current and voltage of stage i in time period j of the process. $\Delta t_{i,j}$ refers to time increment j of the process within stage i.

We used the above performance metrics to compute cost metrics, employing the following simplifying assumptions:

1. We set aside pre-treatment, post-treatment, maintenance and replacement costs, focusing solely on the energy cost and upfront cost of electrodialysis equipment. These costs strongly depend upon feedwater chemistry and can be significant, *e.g.* the cost of basic pre-treatment for waters produced from shale plays, which might involve basic solids removal and/or COD and/or BOD reduction, can fall in the region of \$1/bbl (\$6.3/m^3) [1].
2. We neglect pumping power costs (see Appendix B for justification).
3. We assumed electricity to be priced at K_E = \$0.15/kWh (a conservative estimate of gas pow-

Stage #	Stage 1	Stage 2	Stage 3	Stage 4	Stage 5	Stage 6	Stage 7	Stage 8	Stage 9	Stage 10
Concentrate	230 mS/cm (206,000 ppm)	200 mS/cm (162,000 ppm)	190 mS/cm (150,000 ppm)	180 mS/cm (139,000 ppm)	160 mS/cm (119,000 ppm)	150 mS/cm (109,000 ppm)	130 mS/cm (91,600 ppm)	100 mS/cm (67,200 ppm)	77 mS/cm (50,000 ppm)	52 mS/cm (33,000 ppm)
Initial Diluate	224 mS/cm (195,000 ppm)	192 mS/cm (152,000 ppm)	128 mS/cm (90,000 ppm)	64 mS/cm (40,700 ppm)	32 mS/cm (19,100 ppm)	16 mS/cm (9,010 ppm)	8 mS/cm (4,310 ppm)	4 mS/cm (2,070 ppm)	2 mS/cm (1,010 ppm)	1 mS/cm (492 ppm)
Final Diluate	192 mS/cm (152,000 ppm)	128 mS/cm (90,000 ppm)	64 mS/cm (40,700 ppm)	32 mS/cm (19,100 ppm)	16 mS/cm (9,010 ppm)	8 mS/cm (4,310 ppm)	4 mS/cm (2,070 ppm)	2 mS/cm (1,010 ppm)	1 mS/cm (492 ppm)	0.5 mS/cm (242 ppm)

Figure 2: We designed each of the ten stages such that the diluate conductivity was halved in each successive stage, with the exception of the first two stages. We reduced the salt removal in the first two stages to avoid the depletion of water in the diluate beaker before the end of a trial. We chose concentrate conductivities based on the rates of salt and water transport across the membranes (see Appendix A.1).

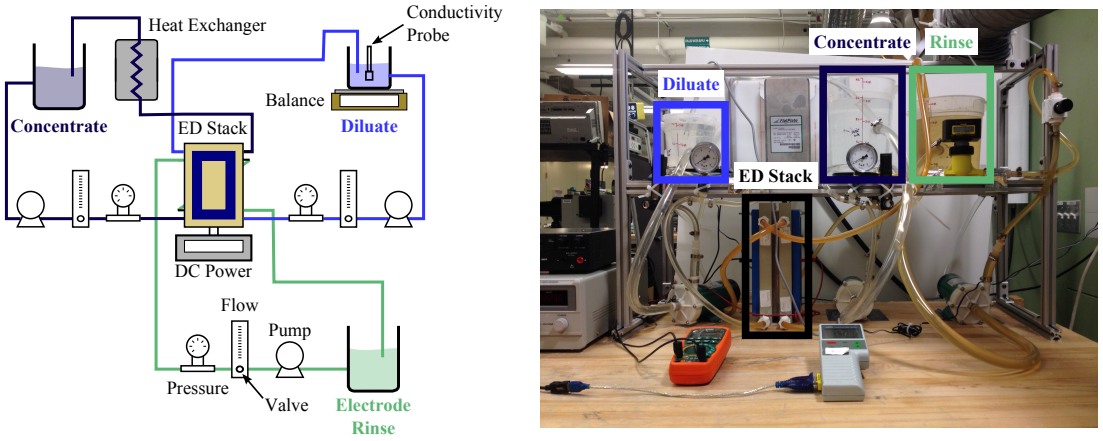

Figure 3: The electrodialysis setup consisted of a diluate, concentrate, and rinse circuit feeding an ED200 stack. We employed a heat exchanger to regulate the temperature of the concentrate, with the stack effectively operating as a second heat exchanger to regulate the diluate temperature. We employed valved-rotameters to regulate the flow rates in each circuit.

ered distributed generation [28]).

4. We assumed equipment costs to scale with membrane area and computed these costs by considering an equipment cost per unit membrane area of $K_Q = 1500$ \$/m^2 (based upon the capital cost data collected by Sajtar and Bagley [29] and analysed by McGovern et al. [21]). This cost data covers plant sizes up to 40000 m^3 per day and feed salinities up to 7,000 mg/L. Its extrapolation to higher salinities is based on the assumption that similar stack designs would be employed at both high and low salinity.

5. We assumed the total installed cost of the equipment to equal three times the estimated equipment costs [30]. This is an estimate since no data exists on commercial scale electrodialysis installations in shale plays.

6. We amortised equipment costs over a twenty-year life, $T = 20$ years, assuming an annualised cost of capital of $r = 10\%$.

Given these assumptions, we defined the specific cost of salt removal, in \$/lb salt (or \$/kg salt) and the specific cost of product water \$/bbl (or \$/m^3) from each stage:

$$\Xi_i^s = K_E E_i^s + \frac{K_Q A_m}{\frac{1}{r}\left[1 - \left(\frac{1}{1+r}\right)^T\right]} \tau_i^s \tag{5}$$

$$\Xi_i^w = K_E E_i^w + \frac{K_Q A_m}{\frac{1}{r}\left[1 - \left(\frac{1}{1+r}\right)^T\right]} \tau_i^w \tag{6}$$

where A_m is the total membrane area in the stack.

2.2. Model

To minimise the cost of salt removal, through optimisation of the stack voltage, we constructed a semi-empirical model for the electrodialysis system, which we validated with experimental results. The process time, energy consumption, and cost of salt removal from each stage were computed using a numerical model that broke each stage into twenty time periods, with an equal change in diluate salinity in each period. During each of these periods the stack voltage and rates of salt and water transport were approximated as constant and used, in conjunction with molar conservation equations, to determine the conditions at the start of the next period. Within each stage, the number of moles of salt and water present in the diluate at the start and the end of each time step j are related to the molar fluxes

of salt and water, $J_{s,j}$ and $J_{w,j}$ and the total cell pair area, A_m:

$$N_{s,j+1} - N_{s,j} = -A_m J_{s,j} \quad (7)$$

$$N_{w,j+1} - N_{w,j} = -A_m J_{w,j} \quad (8)$$

with N_{j+1} and N_j the number of moles of salt, s, or water, w, at the end or start of each time step, A_m the total cell pair area of the stack and J_j the average flux across the membrane area of salt, s, or water, w, at time step j. The concentrate conductivity was approximated as constant in time for each stage and equal to the value employed in experiments. At each instant in time the diluate concentration is approximated as uniform across the membrane area. This is because the time taken for fluid to travel the length of the membrane (<8 s) is much less than the stage processing time (>120 s for all stages).

Salt, water, and charge transport were modelled based upon the approach taken in previous work [31, 32]. Salt transport was modelled by a combination of migration and diffusion:

$$J_s = \left[\frac{T_s^{cp} i}{F} - L_s\left(C_{s,c,m} - C_{s,d,m}\right)\right] \quad (9)$$

and water transport by a combination of migration (electro-osmosis) and osmosis:

$$J_w = \left[\frac{T_w^{cp} i}{F} - L_w\left(\pi_{s,c,m} - \pi_{s,d,m}\right)\right]. \quad (10)$$

In Eq. (10), N_{cp} is the number of cell pairs, T_s^{cp} and T_w^{cp} are the overall salt and water transport numbers for the cell pair, L_s and L_w are the overall salt and water permeabilities of the cell pair, C denotes concentration in moles per unit volume, and π denotes osmotic pressure (calculated employing osmotic coefficients for aqueous NaCl from Robinson and Stokes [33]). The difference between membrane surface concentrations, $C_{s,c,m}$ and $C_{s,d,m}$, and bulk concentrations, $C_{s,c}$ and $C_{s,d}$, was computed via a convection-diffusion based model for concentration polarisation (see Appendix C.1).

The stack voltage was represented as the sum of ohmic terms and membrane potentials:

$$V_{stack} = N_{cp}\left(\bar{r}_{am} + \bar{r}_{cm} + \frac{h_d}{\sigma\Lambda_d C_d} + \frac{h_c}{\sigma\Lambda_c C_c}\right) i + \bar{r}_{cm} i + \frac{2h_r}{\sigma k_r} i + N_{cp}\left(E_{am} + E_{cm}\right) + V_{el} \quad (11)$$

where Λ is the molar conductivity, itself taken to be a function of concentration [34, 35] and h denotes channel height. k denotes electrical conductivity, the subscript r denotes the rinse solution, σ denotes the spacer shadow factor, $\bar{r}$ denotes the membrane surface resistance of the anion or cation exchange membrane and V_{el} denotes the sum of the anode and cathode electrode potentials. Junction potentials associated with concentration differences across boundary layers were neglected while membrane potentials E_{am} and E_{cm} were computed assuming quasi-equilibrium salt and water migration through the membranes (see Appendix C.2).

A series of calibration tests was conducted to establish the values of T_s^{cp}, T_w^{cp}, L_s, L_w, r_m, σ, V_el and the Sherwood number Sh (see Appendix D). Each test was repeated three times to ensure repeatability. Bias errors arising from the determination of the diluate circuit volume (Appendix A.3) and of leakage rates from diluate to concentrate were propagated through the equations defining these nine parameters and combined with the random error [Eq. (12)] that was determined from the sample standard deviation of results computed from the three tests. Errors are computed at a 68% confidence level.

$$\epsilon_{tot}^2 = \epsilon_{bias}^2 + \epsilon_{random}^2 \quad (12)$$

Salt and water transport numbers, T_s^{cp} and T_w^{cp}, were determined via constant current migration tests where the diluate and concentrate conductivities were close to one another. Salt and water permeabilities, L_s and L_w, were determined via diffusion tests with zero current and initial diluate concentrations close to zero. Membrane resistance, r_m, the spacer shadow factor, σ, the electrode potential, V_{el}, and the Sherwood number, Sh, were determined from voltage-current tests at constant diluate and concentrate salinity.

3. Results: Process time, energy consumption and costs

The process time, energy and cost requirements of electrodialysis treatment are shown on a unit salt removal basis in Figs. 4, 5 and 6 and on a unit product water basis in Figs. 7, 8 and 9, in each case illustrating agreement, within error, between the model and the experiment. The deviation between the model and experiment is greatest in the final stages, where the modelled values of energy consumption and process time are highly sensitive to the electrode potential. This is because the driving force for salt transport is the difference between the stack voltage and the sum of the electrode potentials and membrane potentials ($V^{stack} - N_{cp}\left(E_{am} + E_{cm}\right) - V_{el}$). The sum of membrane potentials, $E_{am} + E_{cm}$, scales with the natural logarithm of the salinity ratio (concentrate to diluate) [32] and therefore, in the final stage where the diluate salinity is lowest, the sum of the membrane potentials is greatest — accounting for over 50% of the 8 V applied across the stack. This remaining voltage driving salt transport is therefore highly sensitive to the modelled value of the electrode potential (V_{el}=2.13±0.3 V). This sensitivity further posed a difficulty in modelling desalination, within the final stage, down to 0.5 mS/cm (242 ppm

TDS). The modelled value of the electrode potential (in combination with the modelled values of other fitted parameters, see Appendix D) was such that the back diffusion of salt outweighed salt removal via migration before a conductivity of 0.5 mS/cm was reached. For this reason, the model of the final stage is for an final diluate conductivity of 0.55 mS/cm rather than 0.5 mS/cm.

The trends in process time, energy and cost are most easily explained by considering these quantities on the basis of salt removal. Here we provide scaling estimates that describe the first order variation in process time, energy and cost with stage number. The process time τ for any given stage scales with the change in salinity in that stage ΔS and the inverse of the current I, which describes the number of moles of salt removed per coulomb of charge:

$$\tau \sim \frac{\Delta S}{I} \tag{13}$$

Meanwhile, the current scales approximately with the quotient of the stack voltage over the stack resistance:

$$I \sim \frac{V_{st}}{R_{st}}. \tag{14}$$

The stack resistance scales with the sum of the membrane, concentrate and diluate resistances:

$$R_{st} \sim \left(2r_m + \frac{h}{\sigma k_c} + \frac{h}{\sigma k_d}\right) \tag{15}$$

where σ is the spacer shadow factor, h is the diluate and concentrate channel height, k is the solution conductivity of the diluate d or the concentrate c, and r_m is the anion or cation exchange membrane surface resistance. The process time therefore scales approximately as:

$$\tau \sim \frac{\Delta S}{V}\left(2r_m + \frac{h}{\sigma k_c} + \frac{h}{\sigma k_d}\right). \tag{16}$$

At high diluate conductivity (lower number stages in Fig. 2) the membrane resistance dominates the stack resistance and thus the diluate and concentrate conductivities have a weak effect on process time. At low diluate conductivity (high number stages) the diluate resistance dominates the stack resistance and the process time per unit salt removed scales roughly with the inverse of the diluate conductivity. The stack resistance roughly doubles in moving from one stage to the next and so too does the specific process time.

The energy consumption per unit salt removed, E^s, for any given stage scales with the product of voltage, the current and the process time divided by the change in salinity:

$$E^s \sim \frac{VI\tau^s}{\Delta S}. \tag{17}$$

Considering how process time scales in Eq. (13) it is clear that the energy consumption per unit salt removed scales with the quotient of the voltage over the salt transport number:

$$E^s \sim V. \tag{18}$$

Thus, while process time varies significantly with stage number (note the $\log_2$ scale in Fig. 4) specific energy consumption (plotted on a linear scale in Fig. 5) remains relatively constant.

Given the above explanations for the trends in process time and energy, on the basis of unit salt removal, it is clear that the cost per unit of salt removal must remain relatively constant at low stage numbers (high diluate salinities) but will rise rapidly due to increasing equipment costs at higher number stages (lower salinities) as seen in Fig. 6.

Combining these insights on Fig. 4, 5 and 6 with the fact that salt removal is approximately halved in each stage moving from stage 3 to stage 10 we can easily explain the trends on a basis of stage product water, seen in Fig. 7, 8 and 9. Specific process time on the basis of water produced falls with an increasing stage number because the processing time per unit of salt removed (Fig. 4) rises more slowly than the quantity of salt removed per stage (see Fig. 2). Specific energy consumption, on the basis of product water, falls because energy consumption per unit of salt removed is approximately constant(see Fig. 4) and the quantity of salt removed per stage falls rapidly (see Fig. 2). As a consequence of falling τ^w and E^w with increasing stage number, the specific cost of water also falls in moving to higher stage numbers, primarily because the quantity of salt removed per stage is falling rapidly.

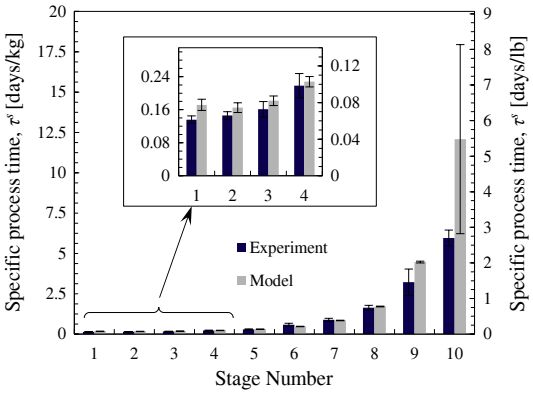

Figure 4: Stage process time per unit of salt removed.

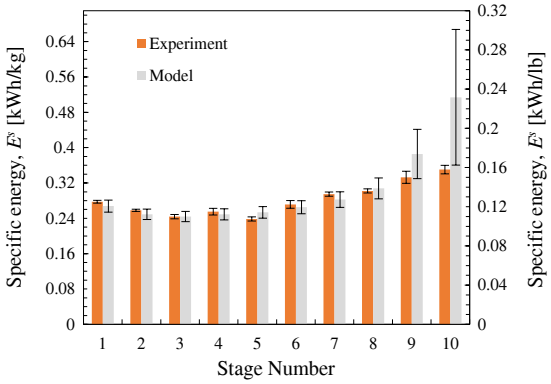

Figure 5: Stage energy consumption per unit of salt removed.

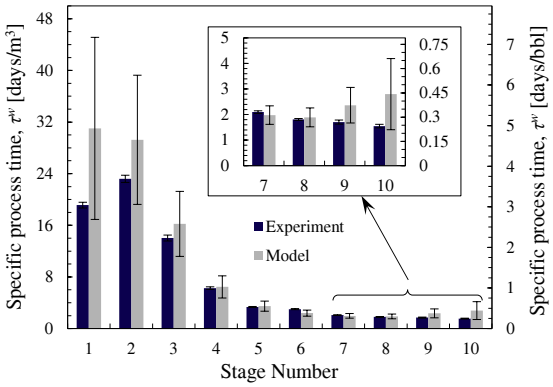

Figure 7: Stage process time per unit of product water.

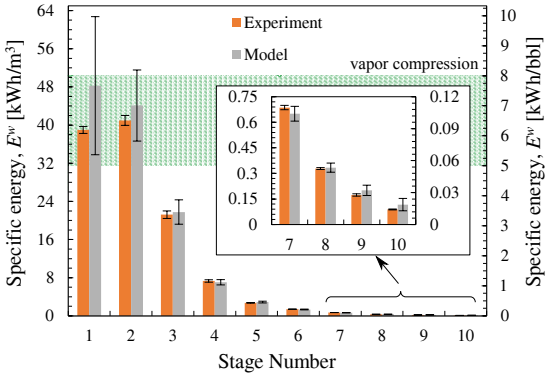

Figure 8: Stage energy per unit of product water. The range of energy consumption for vapour compression is taken from Hayes and Severin for 72.5% recovery of feedwater with TDS of 50,000 mg/L (corresponding roughly to stages 4 through 10) [6].

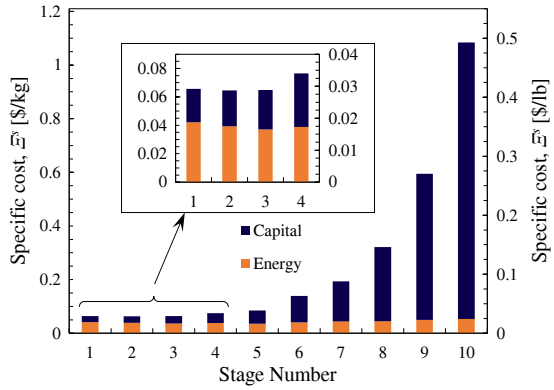

Figure 6: Stage cost per unit of salt removed (based on experimental results).

3.1. Discussion

Not included in the computation of energy in Fig. 5 or Fig. 8 is energy required for pumping, shown in Fig. 10. These values for pumping power are computed via experimental measurements of the pressure drop across the stack and assuming 100% pump efficiency (see Appendix B for detailed calculations). Comparing these values to those for stack energy consumption in Fig. 8, it is clear that pumping power accounts for a significant portion of total power consumption only at low diluate salinity (e.g. stages 10, 9 and 8 where salt removal rates are lowest). Importantly, these values of pumping power for a laboratory scale system are unlikely to be representative of pumping power consumption in a large scale system. This is because the processing length of the system investigated is only 20 cm, meaning that entrance and exit head loss has a disproportionately large effect on the pumping power relative to frictional pressure drop within the membranes, which would be expected to dominate in large scale systems with larger processing lengths.

The range of energy requirements for vapour compression shown in Fig. 8, and of water costs shown in Fig. 9, correspond roughly to a feed salinity equal

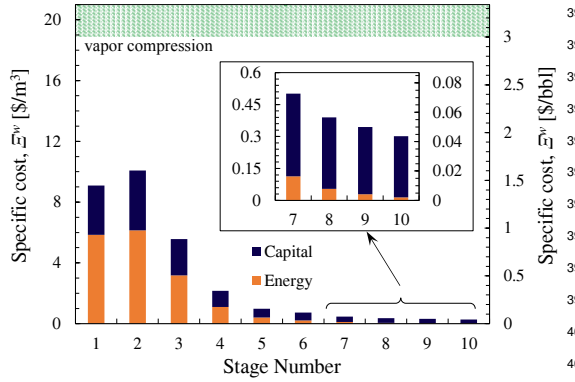

Figure 9: Stage cost per unit of product water (based on experimental results). The range of water costs for vapour compression is taken from Slutz et al., wherein cases are considered with feedwater TDS of 49,500 and 80,000 mg/L (corresponding roughly to stages 4 through 10 and 3 through 10, respectively) [1].

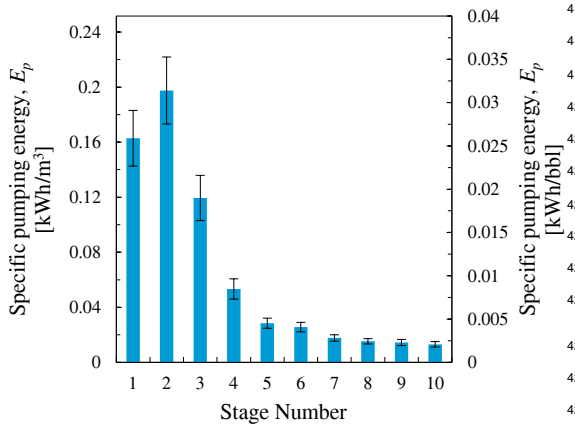

Figure 10: Energy consumption associated with pumping power.

to that of the 3rd or 4th stages of electrodialysis. On this basis, Figs. 8 and 9 indicate that electrodialysis can achieve almost complete salt removal with similar energy requirements and lower water costs than vapour compression [1, 6]. Furthermore, considering electrodialysis costs on the basis of salt removal (Fig. 6), it is interesting that costs fall significantly at higher salinity (*e.g.* in lower number stages). This points to the potential of electrodialysis for the partial desalination of high salinity feed streams.

For electrodialysis systems to be realised for high salinity produced waters, further work is required to address the risks of scaling and fouling. Future work will need to go beyond the simplified solution chemistries considered to date [25, 26], and in this work. Produced waters from shale plays have been shown to contain significant concentrations of dissolved solids with low solubility, including silica, iron, barium and calcium [1, 36]. Furthermore, produced waters may contain significant levels of total organic carbons (up to 160 mg/L, depending on the method used for oil-water separation [37]), while ED manufacturers advise against feedwater total organic carbon concentrations above 15 mg/L [38] *and* a number of studies reveal difficulties in removing total organic carbon with traditional filtration methods [39, 40].

4. Voltage optimisation

Having validated a numerical model for the system we optimise the voltage in each stage to minimise the costs of salt removal. In Fig. 11, we compare three distinct strategies that are shown in Fig. 12:

1. a constant voltage strategy where the voltage is set such that the current density is 80% of its limiting value at the end of stage 10 ($V_{stack,i}$= 16 V, see Fig. A.1);
2. a constant voltage strategy where the voltage is set such that the current density is 50% of its limiting value at the end of stage 10 ($V_{stack,i}$= 8 V, see Fig. A.1); and
3. an optimised strategy where the total costs per stage (equipment and energy) are numerically minimised using a quadratic method [41] to identify an optimal voltage $V^*_{stack,i}$).

Figure 11 reveals that in higher number stages (lower diluate salinities) the strategy of setting the voltage such that the current is just below its limiting value (*e.g.*, 80%) is a good one as this greatly reduces equipment costs. However, at higher salinities (lower stage numbers), it is best to operate with a lower stack voltage that allows for reduced energy consumption. Of course, depending on the relative price of equipment to energy the optimal stack voltage for each stage will differ. Higher electricity prices will drive lower optimal stack voltages and vice-versa. Nevertheless, it is

clear that the brackish water strategy of setting the current close to its limiting value [20] is not necessarily optimal for the treatment of higher salinity waters.

5. Conclusions

Our experimental and economic assessment of electrodialysis at salinities up to 192,000 ppm NaCl indicates good potential for the process at high salinities, such as those seen in produced waters from hydraulically fractured shales. For feedwaters with TDS of roughly 40,000-90,000 ppm, we show that energy requirements are similar and project that combined equipment and energy costs are potentially lower for electrodialysis relative to vapour compression. If partial, as opposed to complete, desalination of a feed water is required, the prospects for ED are even greater as the cost per unit of salt removed is much lower at high diluate salinities. For example, salt removal from a stream of 500 ppm TDS might cost up to four times that of salt removal from a stream at 192,000 ppm TDS per unit of salt removed.

Beyond our experimental assessment of electrodialysis at high salinities, we have developed and validated a numerical model covering a range of diluate salinities from 250 ppm up to 192,000 ppm NaCl. This model reveals the importance of optimising the stack voltage to minimise salt removal costs. For the set of equipment and energy prices examined, we found that brackish water desalination costs are minimised by operating close to the limiting current density, while for salt removal from higher salinity streams lower stack voltages can allow cost reductions of up to 30%.

This analysis addresses two major considerations affecting the viability of ED for the desalination of high salinity produced waters, namely the energy and equipment requirements. Given that ED compares favourably with vapour compression on these metrics a more detailed analysis of an ED system under field conditions is warranted. This might include studies of system fouling and scaling when treating more complex feed waters and an analysis of feedwater pretreatment requirements and costs to ensure robust operation.

6. Acknowledgements

The authors acknowledge support from the King Fahd University of Petroleum and Minerals through the Center for Clean Water and Clean Energy at MIT and KFUPM under project number R15-CW-11. Ronan McGovern and Chester Chambers acknowledge support from the Hugh Hampton Young Memorial Fellowship and partial UROP support from the MIT Energy Initiative, respectively.

7. References

[1] J. A. Slutz, J. A. Anderson, R. Broderick, P. H. Horner, et al., Key shale gas water management strategies: An economic assessment, in: International Conference on Health Safety and Environment in Oil and Gas Exploration and Production, Society of Petroleum Engineers, 2012.

[2] R. Vidic, S. Brantley, J. Vandenbossche, D. Yoxtheimer, J. Abad, Impact of shale gas development on regional water quality, Science 340 (6134).

[3] M. E. Mantell, Produced water reuse and recycling challenges and opportunities across major shale plays, in: Proceedings of the Technical Workshops for the Hydraulic Fracturing Study: Water Resources Management. EPA, Vol. 600, 2011, pp. 49–57.

[4] S. Shipman, D. McConnell, M. P. Mccutchan, K. Seth, et al., Maximizing flowback reuse and reducing freshwater demand: Case studies from the challenging marcellus shale, in: SPE Eastern Regional Meeting, Society of Petroleum Engineers, 2013.

[5] J.-P. Nicot, B. R. Scanlon, R. C. Reedy, R. A. Costley, Source and fate of hydraulic fracturing water in the barnett shale: A historical perspective, Environmental science & technology.

[6] T. Hayes, B. F. Severin, P. S. P. Engineer, M. Okemos, Barnett and appalachian shale water management and reuse technologies, Contract 8122 (2012) 05.

[7] P. Horner, J. A. Slutz, Shale gas water treatment value chain - a review of technologies, including case studies, in: SPE Annual Technical Conference and Exhibition, no. SPE 147264, Society of Petroleum Engineers, 2011.

[8] Proceedings and Minutes of the Hydraulic Fracturing Expert Panel XTO Facilities, Fort Worth September 26th, 2007.

[9] V. Fedotov, D. Gallo, P. M. Hagemeijer, C. Kuijvenhoven, et al., Water management approach for shale operations in north america, in: SPE Unconventional Resources Conference and Exhibition-Asia Pacific, Society of Petroleum Engineers, 2013.

[10] S. Rassenfoss, From flowback to fracturing: water recycling grows in the marcellus shale, Journal of Petroleum Technology 63 (7) (2011) 48–51.

[11] J. Bryant, I. Robb, T. Welton, J. Haggstrom, Maximizing friction reduction performance using flow back water and produced water for waterfrac applications, in: AIPG Marcellus Shale Hydraulic Fracturing Conference, 2010.

[12] A. Kamel, S. N. Shah, Effects of salinity and temperature on drag reduction characteristics of polymers in straight circular pipes, Journal of petroleum Science and Engineering 67 (1) (2009) 23–33.

[13] J. Paktinat, O. Bill, M. Tulissi, Case studies: Improved performance of high brine friction reducers in fracturing shale reserviors, Society of Petroleum Engineers (2011) 1–12.

[14] C. W. Aften, Study of friction reducers for recycled stimulation fluids in environmentally sensitive regions, in: SPE Eastern Regional Meeting, Society of Petroleum Engineers, 2010.

[15] M. J. Zhou, M. Baltazar, Q. Qu, H. Sun, Water-based environmentally preferred friction reducer in ultrahigh-tds produced water for slickwater fracturing in shale reservoirs, in:

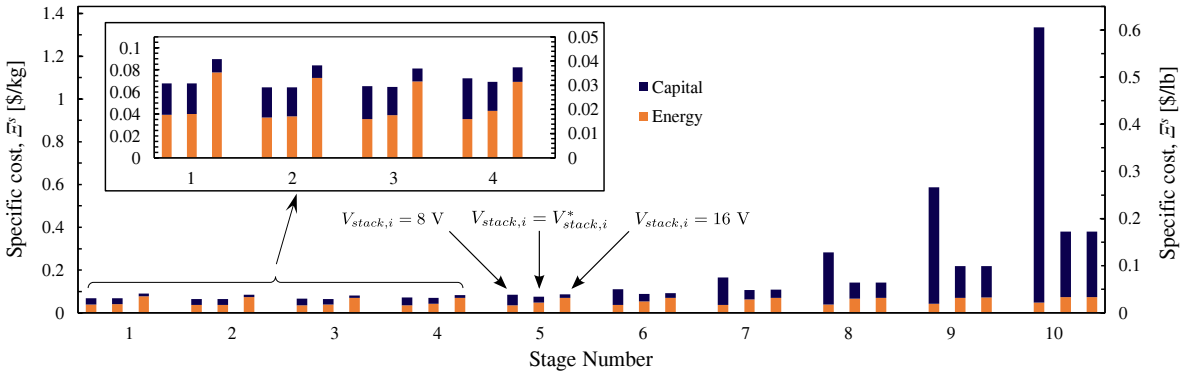

Figure 11: Effect of voltage strategy upon the cost of salt removal.

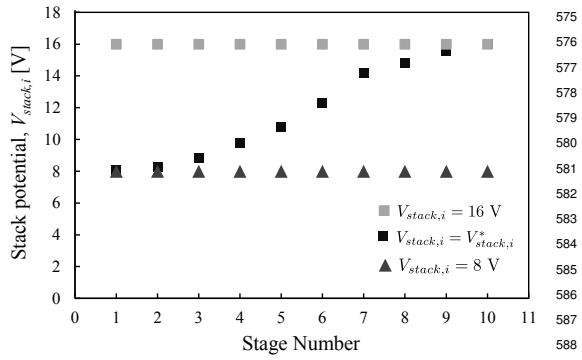

Figure 12: Effect of voltage strategy upon the optimal voltage. At low stage numbers the $V_{stack,i}$= 8 V strategy is close to optimal while at high stage numbers the $V_{stack,i}$= 16 V is closest to optimal.

SPE/EAGE European Unconventional Resources Conference and Exhibition, Society of Petroleum Engineers, 2014.

[16] J. K. Hallock, R. L. Roell, P. B. Eichelberger, X. V. Qiu, C. C. Anderson, M. L. Ferguson, Innovative friction reducer provides improved performance and greater flexibility in recycling highly mineralized produced brines, in: SPE Unconventional Resources Conference-USA, Society of Petroleum Engineers, 2013.

[17] R. LeBas, P. Lord, D. Luna, T. Shahan, Development and use of high-tds recycled produced water for crosslinked-gel-based hydraulic fracturing, in: 2013 SPE Hydraulic Fracturing Technology Conference, 2013.

[18] M. Turek, Dual-purpose desalination-salt production electrodialysis, Desalination 153 (1) (2003) 377–381.

[19] A. Galama, M. Saakes, H. Bruning, H. Rijnaarts, J. Post, Seawater predesalination with electrodialysis, Desalination 342 (2013) 61–69.

[20] H.-J. Lee, F. Sarfert, H. Strathmann, S.-H. Moon, Designing of an electrodialysis desalination plant, Desalination 142 (3) (2002) 267–286.

[21] R. K. McGovern, S. M. Zubair, J. H. Lienhard V, The benefits of hybridising electrodialysis with reverse osmosis, Journal of Membrane Science 469 (2014) 326 – 335.

[22] R. K. McGovern, S. M. Zubair, J. H. Lienhard V, Hybrid electrodialysis reverse osmosis system design and its optimization for treatment of highly saline brines, IDA Journal of Desalination and Water Reuse 6 (1) (2014) 15–23.

[23] T. Brown, C. D. Frost, T. D. Hayes, L. A. Heath, D. W. Johnson, D. A. Lopez, D. Saffer, M. A. Urynowicz, J. Wheaton, M. D. Zoback, Produced water management and beneficial use, Tech. rep., DOE Award No.: DE-FC26-05NT15549 (2009).

[24] M. Turek, Electrodialytic desalination and concentration of coal-mine brine, Desalination 162 (2004) 355–359.

[25] L. Dallbauman, T. Sirivedhin, Reclamation of produced water for beneficial use, Separation science and technology 40 (1-3) (2005) 185–200.

[26] T. Sirivedhin, J. McCue, L. Dallbauman, Reclaiming produced water for beneficial use: salt removal by electrodialysis, Journal of membrane science 243 (1) (2004) 335–343.

[27] PCCell GmbH, ED 200, Lebacher Strasse 60, D-66265 Heusweiler, Germany.
URL `http://www.pca-gmbh.com/pccell/ed200.htm`

[28] R. F. Stiles, M. S. Slezak, Strategies for reducing oilfield electric power costs in a deregulated market, SPE production & facilities 17 (03) (2002) 171–178.

[29] E. T. Sajtar, D. M. Bagley, Electrodialysis reversal: Process and cost approximations for treating coal-bed methane waters, Desalination and Water Treatment 2 (1-3) (2009) 284–294.

[30] M. S. Peters, K. D. Timmerhaus, R. E. West, K. Timmerhaus, R. West, Plant design and economics for chemical engineers, Vol. 4, McGraw-Hill New York, 1968.

[31] M. Fidaleo, M. Moresi, Optimal strategy to model the electrodialytic recovery of a strong electrolyte, Journal of Membrane Science 260 (1) (2005) 90–111.

[32] R. K. McGovern, S. M. Zubair, J. H. Lienhard V, The cost effectiveness of electrodialysis for diverse salinity applications, Desalination 348 (2014) 57–65.

[33] R. Robinson, R. Stokes, Electrolyte Solutions, Courier Dover Publications, 2002.

[34] T. Shedlovsky, The electrolytic conductivity of some uni-univalent electrolytes in water at 25 C, Journal of the American Chemical Society 54 (4) (1932) 1411–1428.

[35] J. Chambers, J. M. Stokes, R. Stokes, Conductances of concentrated aqueous sodium and potassium chloride solutions at 25 C, The Journal of Physical Chemistry 60 (7) (1956) 985–986.

[36] G. P. Thiel, J. H. Lienhard V, Treating produced water from hydraulic fracturing: Composition effects on scale formation and desalination system selection, Desalination 346 (2014) 54–69.

[37] J. M. Silva, Produced water pretreatment for water recovery and salt production, Tech. rep., Research Partnership to Secure Energy for America (2012).

[38] GE Power & Water, GE 2020 EDR Systems (2013).

[39] Q. Jiang, J. Rentschler, R. Perrone, K. Liu, Application of ceramic membrane and ion-exchange for the treatment of the flowback water from marcellus shale gas production, Journal of Membrane Science 431 (2013) 55–61.

[40] M. M. Michel, L. Reczek, Pre-treatment of flowback water to desalination, Monographs of the Environmental Engineering Committee 119 (2014) 309–321.

[41] S. A. Klein, Engineering Equation Solver, Academic Professional V9.438-3D (2013).
[42] M. Fidaleo, M. Moresi, Electrodialytic desalting of model concentrated nacl brines as such or enriched with a non-electrolyte osmotic component, Journal of Membrane Science 367 (1) (2011) 220–232.
[43] A. Sonin, R. Probstein, A hydrodynamic theory of desalination by electrodialysis, Desalination 5 (3) (1968) 293–329.
[44] O. Kuroda, S. Takahashi, M. Nomura, Characteristics of flow and mass transfer rate in an electrodialyzer compartment including spacer, Desalination 46 (1) (1983) 225–232.
[45] E. R. Association, Viscosity of Water and Steam, Edward Arnold Publishers, 1967.
[46] ASTOM Corporation, Neosepta, URL: http://www.astom-corp.jp/en/en-main2-neosepta.html (2013).
[47] K. Kontturi, L. Murtomaki, J. A. Manzanares, Ionic Transport Processes In Electrochemistry and Membrane Science, Oxford, 2008.
[48] N. Berezina, N. Gnusin, O. Dyomina, S. Timofeyev, Water electrotransport in membrane systems. experiment and model description, Journal of membrane science 86 (3) (1994) 207–229.

Nomenclature

Roman Symbols

A_m	cell pair area, m^2
C	concentration, mol/m^3
D	diffusivity, m^2/s
E^s	specific energy of salt removal, kWh/lb or kWh/kg
E^w	specific energy of water produced, kWh/bbl or kWh/m^3
h	channel height, m
i	current density, A/m^2
I	current, A
k	conductivity, S/m
K_E	energy price, \$/kWh
K_Q	area normalised equipment price, \$/m^2 membrane
L_s^{cp}	cell pair salt permeability, m^2/s
L_w^{cp}	cell pair water permeability, mol/m^{2}sbar
m	slope
M	molar mass, kg/mol
m_s	molal concentration, mol/kg w
N	number of moles, mol
N_{CP}	number of cell pairs, -
r	membrane surface resistance, Ω m^2
R	universal gas constant, J/mol K
Re	Reynolds number
Sc	Schmidt number
Sh	Sherwood number
t	process time, s
T	system life, years
$\bar{T}_{cu}$	integral membrane counterion transport number, -
t_{cu}	solution counter-ion transport number, -
T_s^{cp}	cell pair salt transport number, -
T_w^{cp}	cell pair water transport number, -
V_{corr}	stack voltage corrected for concentration polarisation, V
V_{stack}	stack voltage, V
$\mathcal{V}$	volume, m^3
$\dot{\mathcal{V}}$	volume flow rate, m^3/s
w	mass, lbs or kg
x	concentration, mol salt/mol water

Greek Symbols

Δ	change
ϵ	error
Λ	molar conductivity, S m^2/mol
μ	chemical potential, J/mol
ν	viscosity, m^2/s
Ξ^s	specific cost of salt, \$/lb or \$/kg
Ξ^w	specific cost of water, \$/bbl or \$/m^3
π	osmotic pressure, bar
ρ	density, kg/m^3
σ	spacer shadow factor, -
τ^s	specific process time, days/lb or days/kg
τ^w	specific process time, days/bbl or days/m^3

Subscripts

am	anion exchange membrane
c	concentrate
circ	circuit
cm	cation exchange membrane
d	diluate
el	electrode
i	stage number
j	time period
m	membrane surface
p	pump
r	rinse
s	salt
s	water

Superscripts

f	final
in	initial

Appendix A. Determination of experimental conditions

Appendix A.1. Determination of the concentrate salinity in each stage

A key benefit of multi-staging the ED process at high salinities is the possibility of selecting a different concentrate salinity in each stage. If the concentrate salinity were to be the same in all stages it would necessarily be greater than the diluate salinity in the first stage. This would result in very strong salt diffusion from concentrate to diluate and water osmosis from diluate to concentrate in the final stages where the diluate salinity would be much lower than the concentrate. In our experiment we therefore choose higher concentrate salinities in stages with higher diluate salinities and vice versa. In each stage we set the concentrate salinity equal to the steady state salinity that would be dictated by the relative rates of salt and water transport across the membranes:

$$x_{s,c} = \frac{J_s}{J_s + J_w} \tag{A.1}$$

where $x_{s,c}$ is the mole fraction of salt in the concentrate at steady state. To compute each steady-state concentrate value we modelled salt and water transport using the methods of Section 4. Rather than modelling the steady state concentrate salinity for each stage we approximated its value by considering the molar fluxes of salt and water at the very end of each stage.

Since the fitted parameters required for the model were not known a priori, we considered values from the literature for similar ED experiments (Table A.1). Furthermore, in practice an ED system operator may choose to run the stacks with a lower concentrate salinity than could be reached in steady state, perhaps to avoid scale formation. The concentrate salinities chosen for a given application may not exactly match the present study. Nonetheless, the results obtained remain significant as stack performance is primarily affected by the diluate conductivity and membrane resistance rather than concentrate salinity, as explained in Section 3.

Appendix A.2. Selection of the stack voltage

We selected a constant operating voltage of 8 V, which ensured that we never exceeded 50% of the limiting current density during any stage test. We determined the operating voltage from a voltage vs. current test performed at the lowest diluate conductivity (0.5 mS/cm), shown in Fig. A.1.

Appendix A.3. Determination of diluate circuit volume

We determined the diluate circuit volume by measuring the change in salinity (via conductivity) of the diluate solution following the addition of a known amount of salt.

We initially filled the diluate beaker to the 1 L mark with deionised water. We then added a small, known mass of salt, w_s, to the beaker and turned the pumps on. We measured the steady-state conductivity to determine the concentration, C_d in mol/L, of the diluate circuit:

$$C_d = \frac{k_d}{\lambda_d} \tag{A.2}$$

where k_d is the diluate conductivity in S/m and λ_d is the conductance in m^2/Ω equiv. We then converted this concentration to molality, $m_{s,d}$, and solved for the

Symbol	Value	Ref.
Membrane Performance Parameters		
T_s	0.97	[42]
T_w	10	[42]
L_w	8.12×10^{-5} mol/bar-m^2-s	[42]
L_s	5.02×10^{-8} m/s	[42]
$\bar{r}_{am}, \bar{r}_{cm}$	6.0 Ω cm^2	[42]
σ	0.69	[31]
Solution Properties		
D	1.61×10^{-9} m^2/s	[33]
t_{cu}	0.5	[43]
Flow Properties/Geometry		
h	0.7 mm	-
A_m	271 cm^2	-
n_{cp}	17	-
V_{circ}	0.5367 L	-
Sh	20	[42]
Operational Conditions		
V	8 V	-
V_{el}	2 V	[42]

Table A.1: Key parameters used to model salt and water transport across membranes in the electrodialysis stack in order to determine steady-state concentrate salinities for each stage

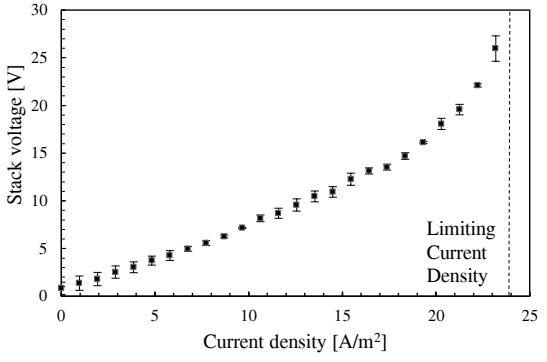

Figure A.1: Voltage vs current test with diluate and concentrate conductivities of 0.5 mS/cm.

volume of the circuit, V_{circ}:

$$V_{circ} = \frac{w_s}{M_s \rho_w m_{s,d}} \tag{A.3}$$

where M_s is the molar mass of salt (kg/mol) and ρ_w is the density of distilled water at 25°C. After repeating the measurement three times, we obtained a diluate circuit volume of 0.54±0.02 L.

Appendix B. Assessment of pumping power

We calculated the required pumping power by measuring the pressure drop in the diluate circuit, ΔP, and multiplying by the diluate flow rate, $\dot{V}$, held at 76 L/hr for each stage. To compute the total pumping power, we assumed the pressure drops in the diluate and concentrate circuits to be equal and multiplied by a factor of two. We discounted the pumping power to drive the rinse circuit since in a large scale system the number of cell pairs per stack is large and hence the ratios of diluate and concentrate flow rates to the rinse flow rate would be small.

We made pressure measurements after flushing the stack with distilled water and operating with diluate, concentrate, and rinse feeds below 500 ppm. Thus we neglected the effect of salinity on density and viscosity. Multiplying by the specific process time of each stage, τ_i, we computed and plotted the specific pumping energy (See Figure 10):

$$E^w_{p,i} = 2\dot{V}\Delta P \tau^w_i \tag{B.1}$$

For the high salinity stages (numbers 5 and below), the specific pumping energy makes up less than 5% of the total specific energy consumed and the contribution to the total specific cost of energy is negligible. In the low salinity stages, the specific pumping energy makes up as much as 40% of the total specific energy consumed. However, this number is largely a characteristic of the small process length of the laboratory scale system used. The relative contribution of stack entrance and exit effects to pressure drop is large relative to frictional pressure drop through the passages between the membranes.

Appendix C. Electrodialysis model

Appendix C.1. Concentration polarisation

The difference between bulk and membrane wall concentrations and osmotic pressures is accounted for by a convection-diffusion model of concentration polarisation:

$$\Delta C = -\frac{\left(\bar{T}_{cu} - t_{cu}\right)}{D} \frac{i}{F} \frac{2h}{\mathrm{Sh}} \tag{C.1}$$

where D is the solute diffusivity, F is Faraday's constant, h is the channel height and t_{cu} is the counter-ion transport number in the diluate and concentrate solutions and is approximated as 0.5 for both anions and cations. $\bar{T}_{cu}$ is the integral counter-ion transport number in the membrane that accounts for both migration and diffusion. It is assumed to be equal in the anion and cation exchange membranes and approximated as:

$$\bar{T}_{cu} \approx \frac{T^{cp}_s + 1}{2}. \tag{C.2}$$

For the a priori calculations of concentrate salinities in Appendix A.1, the Sherwood number is computed using the correlation obtained by Kuroda et al. [44] for spacer A in their analysis:

$$\mathrm{Sh} = 0.5\mathrm{Re}^{1/2}\mathrm{Sc}^{1/3} \tag{C.3}$$

where Sc is the Schmidt number, calculated using the limiting diffusivity of NaCl in water [33] and the kinematic viscosity of pure water ν [45], both at 25°C. Re is the Reynolds number defined as:

$$Re = \frac{2hV}{\nu} \tag{C.4}$$

where V is the mass averaged velocity in the channel.

Appendix C.2. Junction and membrane potentials

Junction potentials associated with concentration polarisation are neglected (which is compatible with taking the transport number of both Na and Cl in solution as 0.5), while the sum of the anion and cation membrane potentials $E_{am} + E_{cm}$ is computed considering quasi-equilibrium migration of salt and water across the membranes:

$$E_{am}+E_{cm} = \frac{T^{cp}_s}{F}(\mu_{s,c,m} - \mu_{s,d,m}) + \frac{T^{cp}_w}{F}(\mu_{w,c,m} - \mu_{w,d,m}) \tag{C.5}$$

where μ_s denotes the chemical potential of salt and μ_w the chemical potential of water; both calculated employing osmotic coefficients and NaCl activity coefficient data from Robinson and Stokes [33]. The subscripts c and d denote the concentrate and diluate while the subscript m denotes a concentration at the membrane surface.

Appendix D. Determination of fitted parameters

Appendix D.1. Sherwood number

The Sherwood number was determined via the limiting current density. A current-voltage test was repeated three times for diluate and concentrate conductivities of 0.5 mS/cm, the results of which are shown in Fig. A.1. The Sherwood number was then determined

by considering the following relationship between it and the limiting current density:

$$i_{lim} = \frac{D_{NaCl} F C_d \mathrm{Sh}}{2h\left(\frac{T_s+1}{2} - t_{cu}\right)}. \quad \text{(D.1)}$$

with D_{NaCl} the diffusivity of sodium chloride in solution, F Faraday's constant, C_d the diluate concentration, h the concentrate and diluate channel heights and T_s the salt transport number. The Sherwood number was found to equal 18±1 (68% confidence).

Appendix D.2. Spacer shadow factor

The spacer shadow factor, σ, quantifies the conductance of the diluate and concentrate channels relative to what the conductance would be were there to be no spacer. When the diluate and concentrate solutions are of high conductivity the stack voltage is insensitive to the spacer shadow factor, since the membrane resistance dominates. Therefore, in determining σ we considered tests where the diluate and concentrate conductivities were low (0.5, 1.5, 2.5 and 7.5 mS/cm). We also considered low values of current density (9.7, 19.3 and 29 A/m^2) where the voltage-current relationship was only weakly affected by concentration polarisation.

The stack voltage data was first corrected (from V_{stack} to V_{corr}) to remove the effects of concentration polarisation, employing the Sherwood number from Appendix D.1 and the model described in Appendix C.1. This allowed the voltage current relationship to be represented by:

$$V_{corr} = (2n_{cp} + 1)i\bar{r}_m + \frac{2Nih}{\sigma k} + \frac{2ih_r}{\sigma k_r} + V_{el} \quad \text{(D.2)}$$

where the terms on the right hand side represent voltage drops across the membranes, the diluate and concentrate (both at the same conductivity), the rinse solutions and the electrodes, respectively. Plotting V_{corr} versus the inverse conductivity of the solution in Fig. D.1 allowed σ to be determined from the slope. Considering:

$$m = \frac{2Nih}{\sigma}, \quad \text{(D.3)}$$

where m is the slope of each of the lines in Fig. D.1, we determined the spacer shadow effect at the three different current densities. Since σ should be independent of current density we computed its value as the average of these three values, giving $\sigma = 0.64 \pm 0.03$.

Appendix D.3. Electrode potential

At low current densities the electrode potential was computed considering the intercept c of each of the lines in Fig. D.1:

$$V_{el} = c - (2N + 1)i\bar{r}_m + \frac{2ih_r}{\sigma k_r}. \quad \text{(D.4)}$$

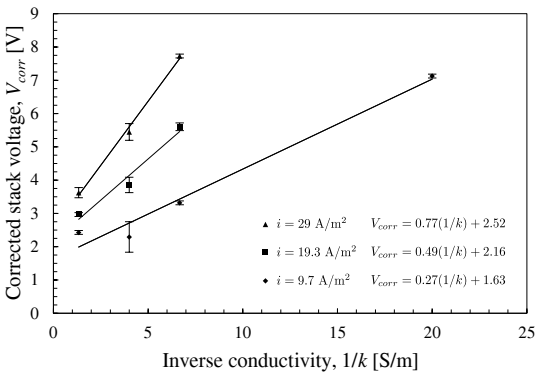

Figure D.1: Determination of spacer shadow effect and electrode potential at low voltage. The markers represent experimental values while the solid lines represent the fitted equations.

At low current densities, the determination of V_{el} is relatively insensitive to the voltage drop across the membranes and the rinse solutions since both are small. Therefore, even though $\bar{r}_m$ is not known a priori, it is reasonable to assume $\bar{r}_m = 3 \times 10^{-4}$ Ω m^2, in line with the membrane resistance quoted by the manufacturer [46]. The values of V_{el} found at 9.7, 19.3 and 29 A/m^2 were 2.4±0.1, 1.9±0.3 and 2.2±0.3, respectively.

To determine the electrode potential at higher current densities, current-voltage tests were carried out with diluate and concentrate conductivities of 25 mS/cm, 75 mS/cm and 150 mS/cm (Fig. D.2). The linearity of these plots at high current densities (above approximately 240 A/m^2) illustrates that neither membrane resistance nor electrode potential is a strong function of current density at high current densities. Furthermore, for these three conductivities, the range of current densities illustrated is far below the limiting current density and the voltage correction for concentration polarisation is thus negligible (*i.e.* $V_{stack} \approx V_{corr}$). The electrode potentials, calculated considering the intercept of the linear fits shown in Fig. D.2 (see Eq. D.2), for data taken at 25 mS/cm, 75 mS/cm and 150 mS/cm were found to be 1.5±0.5, 2.4±0.25 and 2.3±0.4 V, respectively. On the basis of electrode potentials thus being similar at low and high current density, a value of V_{el}=2.13±0.4 V was considered for the model over the entire range of current densities.

Appendix D.4. Membrane resistance

At low diluate and concentrate conductivities the stack voltage is insensitive to the membrane resistance. Thus, we determined the membrane resistance from the high conductivity data of Fig. D.2. The membrane resistance at each value of conductivity was determined using the slope of a linear fit,

$$m = (2N + 1)\bar{r}_m + \frac{2Nh}{\sigma k} + \frac{2h_r}{\sigma k_r}, \quad \text{(D.5)}$$

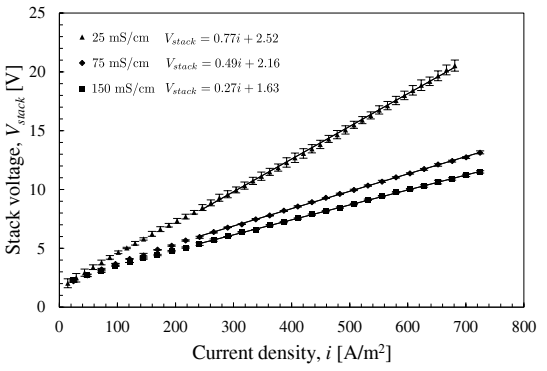

Figure D.2: Determination of membrane resistances and electrode potentials from high conductivity data. The markers represent experimental values while the solid lines represent the fitted equations.

knowing already the value of σ from Appendix D.2. The values of membrane resistance found for solution conductivities of 25 mS/cm, 75 mS/cm and 150 mS/cm were $4.5{\times}10^{-4} \pm 5 \times 10^{-5}$, $2.8{\times}10^{-4} \pm 3 \times 10^{-5}$ and $3.0{\times}10^{-4} \pm 5 \times 10^{-5}$ Ω m^2. Thus, the membrane resistance was modelled as $3.5 \times 10^{-4} \pm 1 \times 10^{-4}$ Ω m^2 over the entire range of diluate and concentrate salinities.

Appendix D.5. Salt and water transport numbers

Salt and water transport numbers at solution conductivities of 7.5 mS/cm, 75 mS/cm, 150 mS/cm and 225 mS/cm were determined by running tests at constant current and measuring the mass of salt and water transported across the membranes in a fixed amount of time. Three tests were performed at each set of conditions to ensure repeatability. During these tests, an approximately constant concentrate conductivity was maintained by selecting an initial concentrate solution volume that was three times that of the diluate. The concentrate beaker was filled with NaCl solution of the desired conductivity and the diluate beaker was filled with NaCl solution that was 1.5, 5, 15 and 15 mS/cm higher than the concentrate conductivity for the 7.5, 25, 75 and 150 mS/cm cases, respectively. The pumps were turned on and a constant current was applied across the stack. The diluate mass and conductivity were recorded until the diluate conductivity reached a value 1.5, 5, 15 and 15 mS/cm below that of the concentrate for the 7.5, 25, 75 and 150 mS/cm cases, respectively. The salt and mass transport numbers were then determined by Eq. (D.6) and Eq. (D.7):

$$T_s^{cp} = \frac{\Delta w_{s,d} F}{n_{cp} I \Delta t M_s} \tag{D.6}$$

$$T_w^{cp} = \frac{\Delta w_{w,d} F}{n_{cp} I \Delta t M_w T_s}. \tag{D.7}$$

Here, $\Delta w_{s,d}$ and $\Delta w_{w,d}$ were the changes in the diluate mass for salt and water respectively, F Faraday's constant, I the applied current across the membrane (10 A), N_{cp} the number of cell pairs, and Δt the process run time. The temperature was held constant at 25°C and the diluate mass was corrected for leakage from diluate to concentrate (determined through leakage tests performed at zero current with deionised water in the concentrate and diluate chambers). Bias errors arising from determining the diluate circuit volume (Appendix A.3) and leakage were propagated through Eqs. (D.7) and (D.6) and combined with the random error [Eq. (12)] that was determined from the sample standard deviation of results from the three tests run at the same conditions. As shown in figure D.3, the salt transport numbers are decreasing with increasing conductivities due to the falling charge density of membranes relative to the solutions [47]. Figure D.4 shows that the water transport numbers are also decreasing with increasing conductivities because of falling water activity, which reduces the membranes' capacity to hydrate [48].

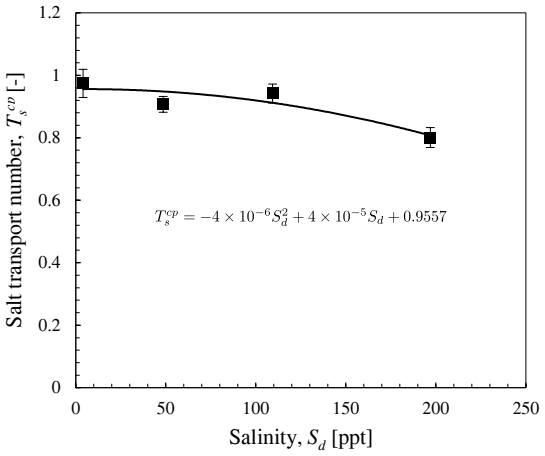

Figure D.3: Salt transport number. The markers represent experimental values while the solid lines represent the fitted equations

Appendix D.6. Salt and water permeability

The permeabilities of the membranes to salt and water at solution conductivities of 7.5 mS/cm, 75 mS/cm 150 mS/cm and 225 mS/cm were determined by running tests at zero current with de-ionised water flowing in the diluate compartment. Three tests were performed at each value of concentrate conductivity to ensure repeatability. During these tests, an approximately constant concentrate conductivity was maintained by selecting an initial concentrate solution volume that was three times that of the diluate. The pumps were turned on and data for diluate conductivity and mass were recorded versus time. Throughout the tests, the temperature was held constant at 25°C. The tests were stopped after the diluate concentration reached conductivities of 200 μS/cm, 900 μS/cm, 900 μS/cm and

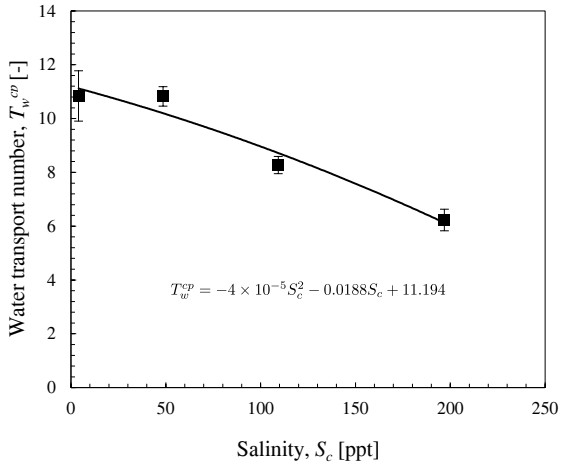

Figure D.4: Water transport number. The markers represent experimental values while the solid lines represent the fitted equations

3,200 μS/cm for the four values of concentrate conductivity respectively. The salt and water permeability coefficients were determined employing Eqns. (D.8) and (D.9)

$$L_s^{cp} = \frac{\Delta w_{s,d}}{(C_c - \frac{\Delta C_d}{2})\Delta t M_s A_m N_{cp}} \quad \text{(D.8)}$$

$$L_w^{cp} = \frac{\Delta w_{w,d}}{\Delta\pi \Delta t M_w A_m N_{cp}} \quad \text{(D.9)}$$

with A_m the active membrane area and N_{cp} the number of cell pairs in the stack. A second order polynomial fit was applied to the salt permeabilities and a power-law fit was applied to the water permeabilities. Bias errors arising from determining the diluate circuit volume (Appendix A.3) and leakage were propagated through Eqs. (D.7) and (D.6) and combined with the random error [Eq. (12)] arising from the sample standard deviation of results from the three tests run at the same conditions.

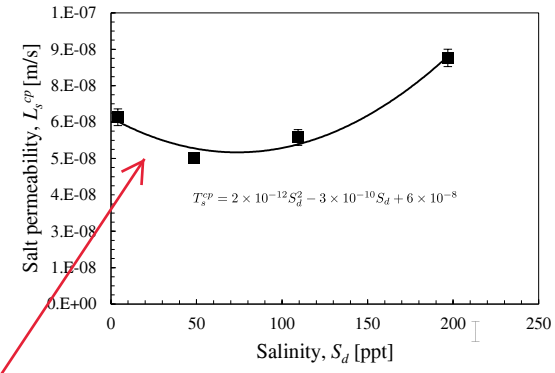

Figure D.5: Salt permeability. The markers represent experimental values while the solid lines represent the fitted equations

The values shown in Fig. D. 5 is the average salt permeability for each membrane and not for the cell pair. Please multiply by 2 for the cell pair salt permeability.

The values shown in Fig. D. 6 is the average water permeability for each membrane and not for the cell pair. Please multiply by 2 for the cell pair water permeability.

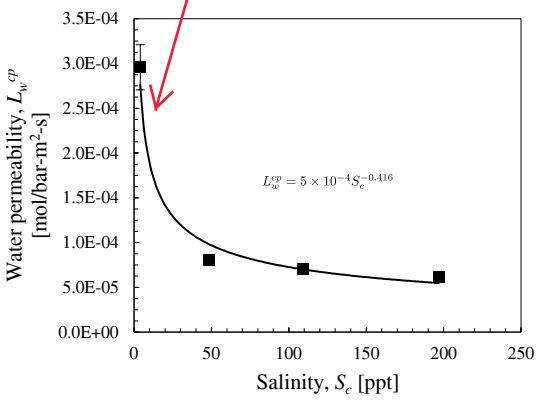

Figure D.6: Water permeability. The markers represent experimental values while the solid lines represent the fitted equations

Appendix D.7. Summary of model parameters

A summary of the model parameters and equations is provided in Table D.2. Membrane salt transport, water transport, salt permeability and water permeability are modelled as:

$$T_s^{cp} = -4 \times 10^{-6} S_d^2 + 4 \times 10^{-5} S_d + 0.96 \pm 0.04 \quad \text{(D.10)}$$

$$T_w^{cp} = -4 \times 10^{-5} S_c^2 - 1.9 \times 10^{-2} S_c + 11.2 \pm 0.6 \quad \text{(D.11)}$$

$$L_s^{cp} = \min(2 \times 10^{-12} S_d^2 - 3 \times 10^{-10} S_d + 6 \times 10^{-8}, 2 \times 10^{-12} S_c^2 - 3 \times 10^{-10} S_c + 6 \times 10^{-8}) \pm 6 \times 10^{-9} [\text{m/s}] \quad \text{(D.12)}$$

$$L_w^{cp} = 5 S_c^{-0.416} \pm 2 \times 10^{-5} [\text{mol/m}^2\text{s bar}] \quad \text{(D.13)}$$

Symbol	Value	Ref.
Solution Properties		
D	1.61×10^{-9} m^2/s	[33]
t_{cu}	0.5	[43]
ν	8.9×10^{-7} m^2/s	[45]
Flow Properties/Geometry		
h	0.5 mm	-
n_{cp}	17	-
Sh	18	-
Membrane Parameters		
σ	0.64±0.03	-
$\bar{r}_m$	3.5×10^{-4}±1×10^{-4} Ω m^2	-
T_s^{cp}	Eq. (D.10)	-
T_w^{cp}	Eq. (D.11)	-
L_s^{cp}	Eq. (D.12)	-
L_w^{cp}	Eq. (D.13)	-
Stack Parameters		
V^{cp}	8 V	-
V_{el}	2.1±0.4 V	-

Table D.2: Electrodialysis Model Parameters

The values for Ls and Lw shown in Eq. D.12 and D.13 are the average permeability for each membrane and not for the cell pair. Please MULTIPLY the given expressions by 2 for the cell pair permeability. The cell pair permeability is twice the average membrane permeability.